EARTHQUAKE ENGINEERING AND STRUCTURAL DYNAMICS, VOL. 21, 95–108 (1992)

SOIL AMPLIFICATION BASED ON SEISMOMETER ARRAY AND MICROTREMOR OBSERVATIONS IN CHIBA, JAPAN

LIN LU, FUMIO YAMAZAKI AND TSUNEO KATAYAMA

Institute of Industrial Science, The University of Tokyo, 7-22-1 Roppongi, Minato-ku, Tokyo 106, Japan

SUMMARY

Soil amplification characteristics of earthquake ground motion were investigated in terms of peak ground acceleration and transfer function based on the Chiba array observation records. The amplification of peak ground acceleration occurred mostly at the top soft layer and was similar for the three components. The effects of non-linear response of soil deposits on the transfer function were examined. Transfer functions calculated by ensemble average were close for the two horizontal components while those obtained from a smoothing operation were generally different. Both the transfer functions from the ensemble average and the smoothing operation underestimated the gain factor around the natural frequencies. A two-step smoothing procedure was proposed and a rotary spectrum was used to improve the estimation of the transfer function. Microtremors were observed at the locations of the boreholes where seismometers are buried. The power spectrum and spatial coherency of the microtremors were compared with those of the earthquake ground motion. Emphasis was placed on the wavetypes which dominated the peaks in the power spectra.

INTRODUCTION

Local site conditions can influence significantly the characteristics of earthquake ground motion, and hence the degree and extent of damage caused by an earthquake. The destruction of structures and ground motions recorded in Mexico City[1,2] from the 1985 Michoacan earthquake and in the San Francisco Bay Area from the 1989 Loma Prieta earthquake[3,4] added more examples to illustrate this fact. Furthermore, the effects of local soil conditions are of particular significance in seismic microzonation, in seismic design of important facilities as well as in seismic safety assessment of existing structures. Thus, investigation of soil amplification characteristics is extremely important.

Both local topographical and geological conditions can generate significant amplifications and spatial variations of the earthquake ground motion. In recent years, a large number of seismograph arrays[5–9] have been installed in various places in the world in order to investigate these effects. However, since strong motion earthquakes do not occur often, it may take some time until comprehensive studies can be conducted using observed data from these arrays.

Microtremor observation[10–13] is another popular tool to assess the effect of soil conditions in earthquake engineering. It is also utilized often to evaluate natural periods of structures. Microtremors embody a wide range of frequency contents and can be measured at any time and for any duration. The differences in source, propagation path and vibration amplitude between a microtremor and earthquake ground motion necessitate further study on the application of microtremors to earthquake engineering.

This paper attempts to investigate soil amplification characteristics using strong motions recorded from a unique three-dimensional array[14] in Chiba, Japan. It also analyses the spectral characteristics of the microtremors measured at 11 points in the ground surface of the same array and the results are compared with those of the earthquake ground motion.

CHIBA SEISMOMETER ARRAY AND ITS STRONG MOTION DATABASE

Since 1982, a dense seismometer array[14] has been in operation in the Chiba Experiment Station of the Institute of Industrial Science, the University of Tokyo. The Chiba station is located about 30 km east of

0098–8847/92/020095–14$07.00

Received 8 July 1991
Revised 27 August 1991

Tokyo with the longitude 140°6′37″E and the latitude 35°37′17″N. In this array, 44 accelerometers are placed very densely in 15 boreholes in an area of about 300 m × 300 m, as shown in Figure 1. It should be noted that boreholes C1 to C4, which are only 5 m from borehole C0, are not marked in Figure 1. In each borehole, the accelerometers are buried at different depths, i.e. 1, 5, 10, 20 and 40 m from the ground surface. The topographical and geological conditions of the array site are basically simple and the ground surface is generally flat. Figure 2 shows the typical soil profile of the site at borehole C0.

To date, more than 160 earthquakes have been recorded in this array, although most of the recorded events are rather weak. Recently, the Chiba array database[14] was developed from ground motions of 27 major events having peak ground accelerations at the ground surface generally greater than 20 cm/s^2. Information about these 27 events is listed in Table I.

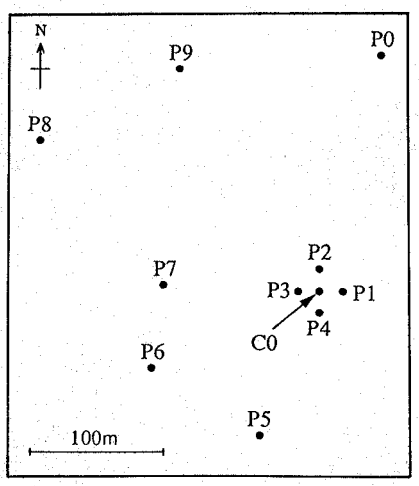

Figure 1. Layout of boreholes in Chiba array

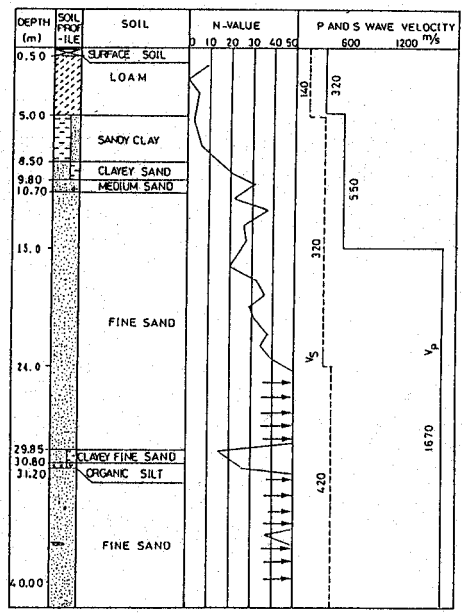

Figure 2. Soil profile at borehole C0

Table I. Information on the earthquake records

No.	Date	JMA magnitude	Epicentral dist. (km)	Focal depth (km)	Max. acc. at C001 (cm/s^2)	Location of Epicentre
1	23/07/82	7·0	178	30	28·3	Off Kanto
2	27/02/83	6·0	35	72	55·7	Southern Kanto
3	01/01/84	7·3	373	388	25·5	South off Kinki
4	06/03/84	7·9	702	452	28·0	near Torishima
5	14/09/84	6·8	232	2	4·5	West Nagano Pref.
6	19/09/84	6·6	219	13	14·5	Southeast off Kanto
7	17/12/84	4·9	5	78	24·1	Tokyo Bay region
*8	08/06/85	4·8	16	64	29·6	central Chiba Pref.
*9	04/10/85	6·1	28	78	82·2	South Ibaragi Pref
*10	06/11/85	5·0	32	63	75·7	Southern Boso Pen.
*11	12/02/86	6·1	125	44	15·4	East off Ibaragi Pref.
*12	24/06/86	6·5	105	73	54·0	Southeast off Boso Pen.
13	22/11/86	6·0	131	15	6·0	near Izu-Oshima Island
14	06/02/87	6·7	219	35	14·0	East off Fukushima Pref.
*15	30/06/87	4·9	62	57	33·5	Southwest Ibaragi Pref.
*16	17/12/87	6·7	45	58	327·1	East off Chiba Pref.
*17	17/12/87	4·6	46	52	21·2	East off Chiba Pref.
*18	17/12/87	4·4	42	58	23·8	East off Chiba Pref.
19	17/12/87	4·0	52	42	30·4	East off Chiba Pref.
*20	05/01/88	4·2	37	42	40·8	East off Chiba Pref.
*21	16/01/88	5·2	38	48	97·8	East off Chiba Pref.
22	18/01/88	4·1	17	32	26·2	Tokyo Pref.
*23	18/03/88	6·0	42	96	59·8	Tokyo Pref.
*24	12/08/88	5·3	62	69	46·4	Southern Chiba Pref.
*25	19/02/89	5·6	48	55	55·7	Southwest Ibaragi Pref.
*26	06/03/89	6·0	55	56	28·9	Northern Chiba Pref.
*27	11/03/89	4·9	52	45	41·0	Southern Ibaragi Pref.

Events with * were used for ensemble average of transfer function.

SOIL AMPLIFICATION FROM EARTHQUAKE RECORDS

Amplification of peak ground acceleration

The amplification of peak acceleration was examined from ground motions at borehole C0 recorded at the depths of 1, 5, 10, 20 and 40 m from the ground level (GL). The recorded peak accelerations at GL − 1, − 5, − 10 and − 20 m were normalized by those at GL − 40 m for the 27 events. The ratios for the three components, i.e. the East–West (EW), North–South (NS) and Up–Down (UD) for individual events are shown in Figure 3. Although the peak acceleration alone does not indicate the degree of damage due to an earthquake, it is used commonly to represent the intensity of ground motion.

The amplification took place mostly within a few metres below the ground surface. From the soil profile of borehole C0 (Figure 2), it is seen that the soil stiffness of the top 5 m is much softer than that of the underlying layer. Such amplification is considered to be caused by this soft layer. It was noticed at the Chiba array site that the amplification ratio of peak acceleration for the vertical component is rather close to those of the horizontal components although the peak accelerations of the different components usually occurred at different moments and were dominated by different wave types.

The amplification ratios were scattered among the events and it is rather difficult to explain this scatter by the characteristics of each event, e.g. the magnitude, epicentral distance and focal depth. But generally, the peak acceleration increased as the seismic wave propagated upward. One exception was the 1984 West Nagano Prefecture earthquake (#5 in Table I), in which almost no amplification was observed for all the three components. The surface wave was found to be dominant in this event.[15]

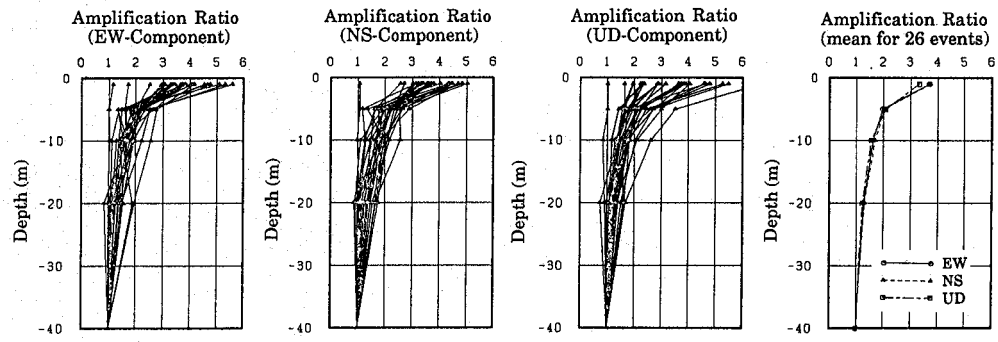

Figure 3. Amplification ratios of peak ground acceleration for 27 events at borehole C0

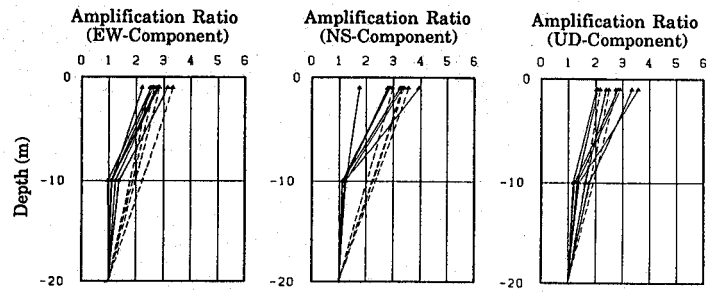

Figure 4. Amplification ratios of peak ground acceleration at 11 boreholes for the 1985 South Ibaragi Prefecture earthquake

Amplification ratios were also calculated for the ten P-series boreholes (refer to Figure 1) for the 1985 South Ibaragi Prefecture earthquake (#9) as shown in Figure 4. The amplification ratios at GL − 1 m with respect to those at GL − 20 m ranged from about 2 to 4 although soil conditions are rather similar for these boreholes.

The averages of the amplification ratios at the different depths for the 26 events were calculated excluding the 1984 West Nagano Prefecture event. While the amplification ratio differed for the two horizontal components of an individual event, the averages were almost equal for all depths, as shown in Figure 3. The average of the amplification ratios at GL − 1 m was about 3·7 and that at GL − 5 m about 2. This means that the peak acceleration at GL − 5 m was about half that at the ground surface. In contrast, there was almost no amplification from GL − 40 to GL − 20 m.

Spectral characteristics of soil amplification

The spectral characteristics of soil amplification were investigated in terms of transfer function $H(f)$:

$$H(f) = \frac{S_{xy}(f)}{S_{xx}(f)} \tag{1}$$

where $S_{xx}(f)$ is the power spectrum of the input motion and $S_{xy}(f)$ is the cross spectrum of input and output motions. The ensemble average from 16 events was used to estimate these spectra statistically while a smoothing technique was employed with a Parzen window of 0·4 Hz bandwidth to estimate these spectra from a pair of ground accelerations. These 16 events, asterisked in Table I, have relatively larger peak values and longer durations than the others. In the case of the ensemble average, the power spectra of output motions were normalized by the area of $S_{xx}(f)$ owing to the large power difference of each event.

Before taking the ensemble average, possible effects of non-linear response of soil deposits on the transfer function were examined. This was conducted by comparing the transfer functions calculated from the records

of the 1987 East off Chiba Prefecture earthquake (# 16), which had the strongest ground motion recorded at the site, and for event # 18, which is one of its aftershocks. The former had a peak acceleration of 327 cm/s^2 on the ground surface while the latter had a peak acceleration of 24 cm/s^2. The transfer functions for these two events at borehole C0 by smoothing are shown in Figure 5. The transfer functions of GL – 1/GL – 5 m and GL – 1/GL – 10 m exhibited some shifts in natural frequencies while the amplitude remains almost the same. This effect was not shown clearly in the other two transfer functions (GL – 1/GL – 20 m and GL – 1/GL – 40 m). Therefore it may be considered that the effect of the non-linear response is small for the selected 16 events as far as the transfer functions of GL – 1/GL – 20 m and GL – 1/GL – 40 m are concerned. Thus, they can be used for computing the ensemble average.

The ensemble transfer functions calculated from the records at GL – 1 and GL – 20 m in borehole C0 for the 16 events are shown in Figure 6. Although the results of the ensemble averages were not smooth enough because of the limited number of samples, the spectral characteristics of soil amplification can be observed clearly. Amplification of about 6 was found at the frequencies of about 4 and 7·5 Hz for the two horizontal ground motions. The change of phase angle around the natural frequencies was steep, indicating small damping.

The transfer functions obtained from the ensemble average were very similar for the two horizontal components but different for the vertical component. The difference seemed to be caused by different dominant wave types. Usually, the S-wave is dominant in the horizontal motion while the P-wave is

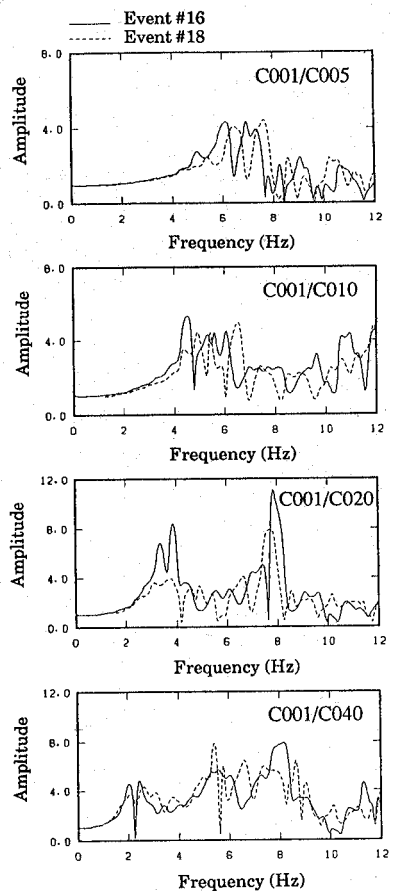

Figure 5. Transfer functions estimated from NS component of the 1987 East off Chiba Prefecture earthquake and one of its aftershocks in borehole C0

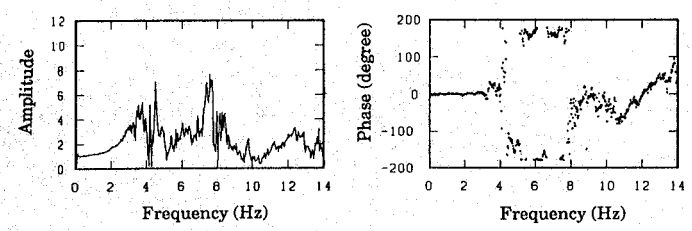

(a) EW Component

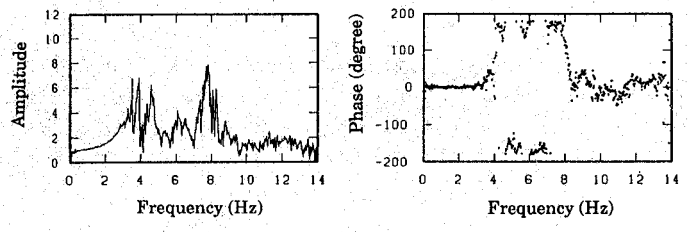

(b) NS Component

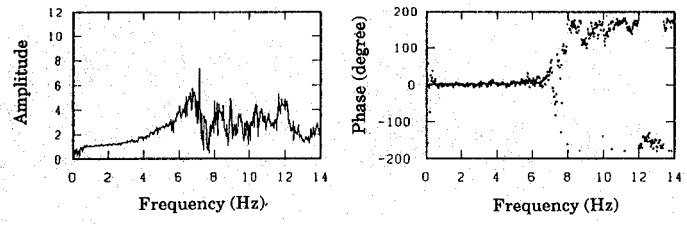

(c) UD Component

Figure 6. Ensemble transfer functions from 16 events for GL − 1/GL − 20 m in borehole C0

dominant in the vertical motion. The similar shape and the close value of the two horizontal components indicate that the site does not show directivity to the amplification of the shear wave.

There were sharp valleys in the transfer functions near the natural frequencies. The valleys may be attributed partly to the average of the cross spectrum $S_{xy}(f)$. It is known that the phase angle of a transfer function changes sharply around the natural frequencies. Therefore, the phase angle near the natural frequency is very sensitive to small variations in the stiffness of the system and to slight randomness of input. In fact, the phase angles from the 16 events were highly scattered around the natural frequencies. The average of complex numbers is usually computed by taking the averages for the real part and for the imaginary part. Thus, the scattered phase angles have a considerable effect on the averaged amplitude of $S_{xy}(f)$. Although equation (1) generally gives a good estimate of the transfer function,[16] it should be pointed out that the amplitude of this estimated transfer function near natural frequencies is often much smaller than the actual amplification of the site.

Power spectra for the records at GL − 1 m were calculated individually for the 16 events. These were normalized by their respective maximum values as shown in Figure 7 because the powers vary for the 16 events. Although the transfer functions estimated for the 16 events looked similar, considerable differences were observed among the power spectra at the ground surface. This means that the spectral characteristics were also influenced by the input to the surface layer, which may vary depending on the fault mechanism and the travel path. It was found that low frequency contents were more dominant in large-magnitude events than in small-magnitude ones.

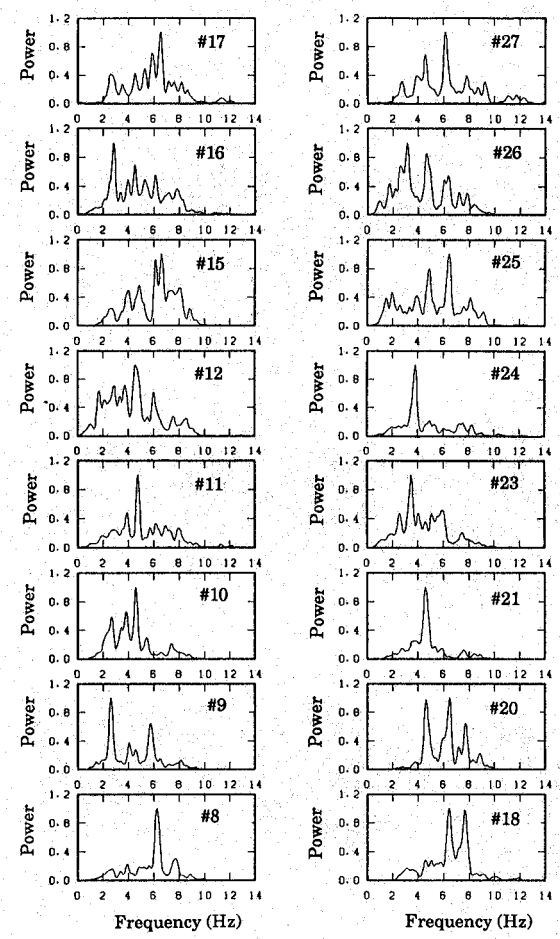

Figure 7. Normalized power spectra of the records on the ground surface for NS components from 16 events

A two-step smoothing procedure

A smoothing procedure is often used to estimate transfer functions from a single event because of the limited number of ground motion records. Transfer functions for each of the 16 events were also estimated by smoothing. Figure 8 shows the resulting transfer function from the records at GL − 1 and GL − 20 m for the 1985 South Ibaragi Prefecture earthquake (#9). These were generally in agreement with those from the ensemble average. However, the two horizontal components were somewhat different. Sharp valleys occurred near the natural frequencies. The sharp valley means that the ground motion at these frequencies was less amplified than that at its neighbouring frequencies. On the contrary, the amplification at the natural frequencies is demonstrated clearly by comparing the waveforms of the input and output motions. Figure 9 shows the filtered acceleration time histories at GL − 1 m and that at GL − 20 m in borehole C0 during the South Ibaragi Prefecture event. The waveforms were for the frequency contents from 3·85 to 4·15 Hz (the natural frequency is around 4·0 Hz). While a sharp valley in the EW component is observed around 4 Hz in Figure 8, considerable amplification is seen in Figure 9.

The underestimation of the amplitude of the transfer function around the natural frequencies is due partly to the smoothing operation on cross spectrum S_{xy} (f). The effect of smoothing on the transfer function was demonstrated by an equivalent linear earthquake response analysis for the Chiba array site.[17] As a result, a two-step smoothing procedure was proposed to improve the valleys.

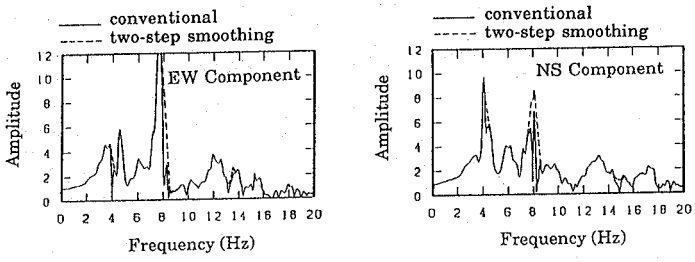

Figure 8. Comparison of transfer functions for GL − 1/GL − 20 m obtained by smoothing operations

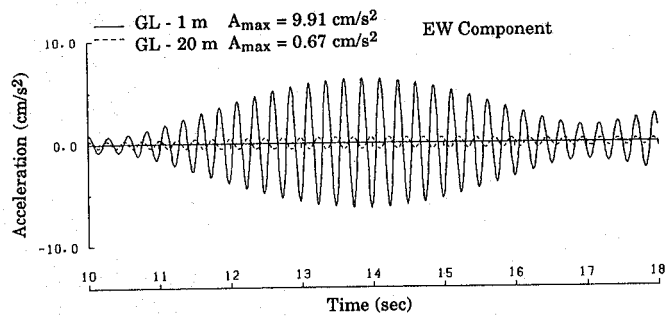

Figure 9. Filtered motions for the frequencies between 3·85 and 4·15 Hz at GL − 1 and GL − 20 m

The cross spectrum $S_{xy}(f)$ can be written as

$$\tilde{S}_{xy}(f) = \tilde{u}(f) + \mathrm{i}\tilde{v}(f) = \tilde{A}_{xy}(f)\mathrm{e}^{-\mathrm{i}\tilde{\theta}_s(f)} \tag{2}$$

where $u(f)$ and $v(f)$ are the real part and the imaginary part, respectively, and $A_{xy}(f)$ and $\theta_s(f)$ are the amplitude and phase angle, respectively, and the tilde indicates the smoothed value. Some randomness may be included in $S_{xy}(f)$ when it is calculated from earthquake records. Therefore, before smoothing, $S_{xy}(f)$ can be written as

$$S_{xy}^{(0)}(f) = u^{(0)}(f) + \mathrm{i}v^{(0)}(f) = A_{xy}^{(0)}(f)\mathrm{e}^{-\mathrm{i}[\tilde{\theta}_s(f) + \theta_r(f)]} \tag{3}$$

where $\theta_r(f)$ represents the random phase angle.

Because the conventional smoothing operation has been found as having little effect on the estimation of $\theta_s(f)$, the phase angle $\theta_s(f)$ is, as the first step, estimated by

$$\tilde{\theta}_s(f) = \arctan\frac{\tilde{v}^{(0)}(f)}{\tilde{u}^{(0)}(f)} \tag{4}$$

Once the phase angle $\theta_s(f)$ is estimated, it is removed from equation (3) in order to obtain the amplitude $A_{xy}(f)$ correctly. By eliminating $\theta_s(f)$ from equation (3), it becomes

$$S_{xy}^{(1)}(f) = u^{(1)}(f) + \mathrm{i}v^{(1)}(f) = A_{xy}^{(0)}(f)\mathrm{e}^{-\mathrm{i}[\theta_r(f)]} \tag{5}$$

Applying the smoothing operation to equation (5) as the second step, the amplitude $A_{xy}(f)$ is obtained by

$$\tilde{A}_{xy}(f) = \sqrt{[\tilde{u}^{(1)}(f)]^2 + [\tilde{v}^{(1)}(f)]^2} \tag{6}$$

In this way, the cross spectrum is determined from the phase angle $\theta_s(f)$ estimated in the first smoothing step and from the amplitude $A_{xy}(f)$ calculated by the second smoothing step. The transfer functions estimated by applying the two-step smoothing procedure on the cross spectrum are shown in Figure 8. It can be noticed that the sharp valleys near the natural frequencies were improved.

Rotary spectrum

As mentioned earlier, the smoothing procedure gives dissimilar transfer functions for the two horizontal components while the ensemble average gives similar functions. This difference in transfer functions obtained from smoothing may lead to confusion in some cases. This difference can be eliminated by using the rotary spectrum.[9,18] Consider both an input motion $w(t)$ and an output motion $z(t)$ are defined by vectors consisting of two horizontal components as

$$w(t) = x_1(t) + ix_2(t) \quad \text{and} \quad z(t) = y_1(t) + iy_2(t) \tag{7}$$

where $x_1(t)$ and $y_1(t)$ represent the EW component and $x_2(t)$ and $y_2(t)$ mean the NS component of ground motion. The auto and cross rotary spectra are calculated by

$$S_{ww}(f) = \frac{1}{4}\{S_{x_1x_1}(f) + S_{x_2x_2}(f) + 2\mathrm{Im}[S_{x_1x_2}(f)]\} \tag{8}$$

$$S_{wz}(f) = \frac{1}{4}\{S_{x_1y_1}(f) + S_{x_2y_2}(f) + i[S_{x_1y_2}(f) + S_{x_2y_1}(f)]\} \tag{9}$$

Instead of calculating the spectra for individual components, the rotary spectrum is calculated by taking the two components as a complex number. Hence the resultant transfer function becomes like an average of those for two horizontal components. Figure 10 shows the transfer function calculated by introducing the rotary spectrum together with the proposed two-step smoothing procedure. The transfer function was very close to those obtained by ensemble average except for the valleys near the natural frequencies (Figure 6). It is believed that the transfer function near the natural frequencies shown in Figure 10 represents more realistic soil amplification characteristics.

MEASUREMENT AND ANALYSIS OF MICROTREMOR

Measurement of microtremor

Microtremor was measured at 11 points on the ground surface of the Chiba array site. These points corresponded to the locations of boreholes C0, P1 to P0 shown in Figure 1. Velocity type pickups each having a natural frequency of 2 s and a viscous damping ratio of 0·64 were used. Characteristics of the available eight horizontal and four vertical pickups were calibrated by shaking table tests before the measurement.

Microtremor was observed from 10:30 pm (local time) of 26 April 1990 to 4:30 am of the following day. It was a fine night with a gentle breeze. Because of the limited number of pickups, the 11 points were not measured simultaneously. Instead, measurements were taken for 6 sets of 2 to 4 points at a time. Recordings were made in terms of velocity and displacement for more than 5 min at each point in the three directions, i.e. East–West, North–South and Up–Down directions. The signals were recorded on a magnetic tape every 0·01 s by a 64-channel digital recorder, the same type being used for the seismometer array system. However, only a 1 min stationary part was chosen from the 5 min observation and was used for the analysis because some evident noise was recorded.

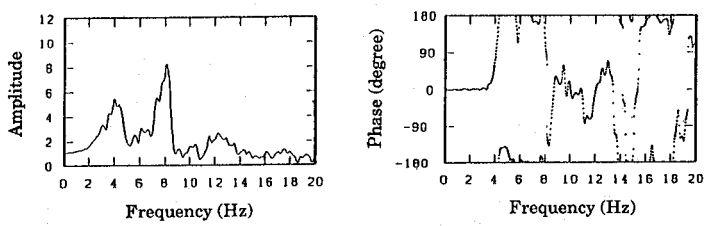

Figure 10. Transfer function (GL − 1/GL − 20 m) estimated by using both the rotary spectrum and the two-step smoothing procedure

Microtremors were compared with the earthquake ground motion in terms of their velocity. The ground motion records from the 1985 South Ibaragi Prefecture earthquake were used for the comparison because records were complete for all the 11 boreholes. The velocity of the earthquake ground motion was obtained by integrating the recorded acceleration time history. Figure 11 compares an example of the time histories from microtremor and earthquake ground motion for the three components. The microtremors look stationary while the earthquake motions show time dependent wavetypes and frequency content.

Power spectrum

The power spectrum was calculated for both the microtremors and the earthquake ground motions by applying the smoothing operation with the Parzen window of 0·4 Hz bandwidth. Durations of the records used for the analysis were 40 s for the earthquake records and 1 min for microtremor. The power spectra for the three components of microtremor and the 1985 South Ibaragi Prefecture event at borehole P1 are shown in Figures 12(a) and (b), respectively.

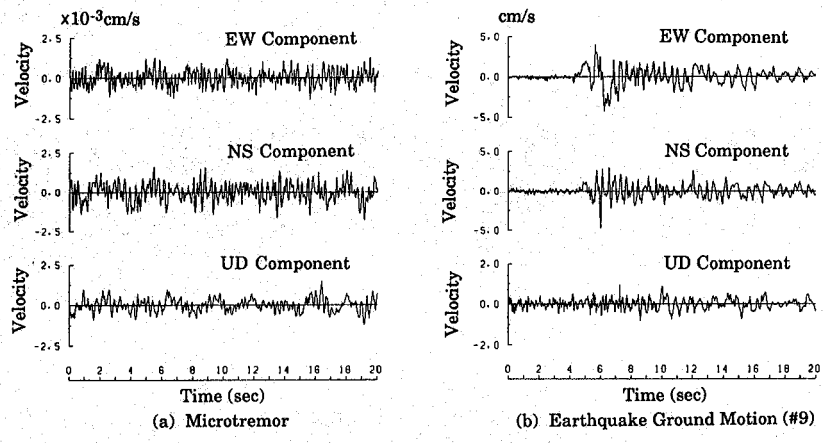

Figure 11. Velocity time histories of microtremor and earthquake ground motion at borehole P1

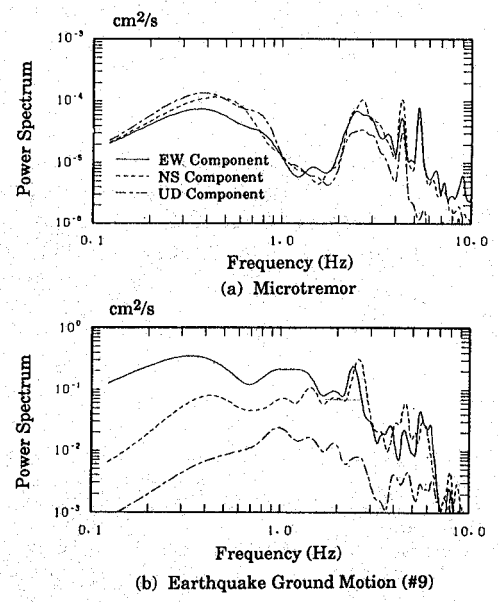

Figure 12. Power spectra of microtremor and an earthquake event for the three components at borehole P1

For the microtremor, the power spectra of the three components showed similar shapes. In the case of the earthquake records, the power spectrum of the vertical component was considerably different from those of the horizontal components. The power of the earthquake ground motion came mainly from the S-wave for the horizontal components and from the P-wave for the vertical component. But for the microtremor, all the three components may have originated from similar sources. Thus, the vertical component of the microtremor contains almost the same information as the horizontal components. The power spectra of the two horizontal components of this event showed a significant discrepancy for frequencies less than 1 Hz. However, this difference between the horizontal components was not always observed in other events.

The power spectra calculated for the three stronger records in the Chiba array database (#9, #16 and #27 in Table I) along with that of the microtremor at borehole P1 are shown in Figure 13. To have a clear comparison, the power spectra were normalized by each respective area. The spectrum of the microtremor showed its first peak at about 0·4–0·6 Hz and the second peak at about 2·5 Hz. There were other peaks at frequencies higher than 4 Hz. The spectra of earthquake motions showed a peak at around 0·4 Hz for some events and distinct peaks at around 2·5 Hz for all the three events. The agreement of the peaks of the spectra of microtremor and earthquake motions around 2·5 Hz can be observed.

Figures 14 (a) and (b) show the power spectra of the microtremor and earthquake ground motion (#9), respectively, at the 11 points. The 11 power spectra for earthquake ground motion showed better similarity

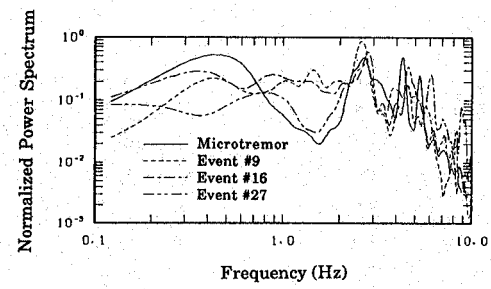

Figure 13. Power spectra of microtremor and three earthquake events for the NS component at-borehole P1

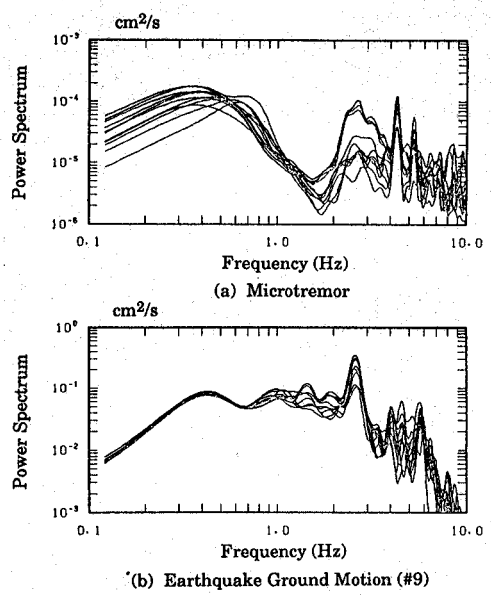

Figure 14. Power spectra of microtremor and earthquake ground motion for the NS component at the 11 locations

than those for the microtremor. The difference of power spectra for the earthquake event at different points might have been caused primarily by the difference in soil conditions. It should be noted that records for the microtremor were not simultaneously measured at all 11 points, which might cause the difference in the power spectra.

From the results of the soil amplification investigation, it was concluded that 2·5 Hz corresponds to the natural frequency for the soil layers down to a depth of about 40 m in the Chiba site. This frequency was also found to affect the spectral characteristics of earthquake ground motions at the ground surface considerably.

Apparent wave velocity

The wavetypes which contributed considerably to the peaks around 0·4–0·6 and 2·5 Hz were investigated further by means of the apparent wave velocity calculated by the tripartite method. Using the vertical component observed at the locations of boreholes C0, P5 and P6, the apparent wave velocity for the frequency content in the frequency range from 0·5 to 0·7 Hz, corresponding to the peak (0·6 Hz) measured in these three points, was obtained to be about 460 m/s. The dispersion curve for the Rayleigh wave can be calculated[19] theoretically by modelling the site composed from several horizontal layers. Using the layered model[15] of the Chiba site, the dispersion curve for the Rayleigh wave of the fundamental mode was obtained and is shown in Figure 15. It was found that the apparent wave velocity calculated from the tripartite method for the microtremor is very close to the phase velocity of the Rayleigh wave. Thus, the first peak of the microtremor may be concluded to be the Rayleigh wave.

The tripartite method was utilized further for the microtremor at the frequency content from 2·4 to 2·6 Hz, covering the frequency range of the peak around 2·5 Hz. An apparent wave velocity of 1320 m/s was obtained from the NS components recorded at boreholes C0, P5 and P6. The incident angle was estimated at about 6 degrees with the vertical axis. Since the apparent wave velocity of the microtremor is large and the power of the horizontal components is stronger than that of the vertical component for the frequency content corresponding to the peak of about 2·5 Hz, the wave of the microtremor between 2·4 to 2·6 Hz may be the S-wave propagating through the site upward. Hence, the coincidence of the peaks of power spectra around 2·5 Hz for both microtremor and earthquake ground motion may indicate that both are due to the local soil effect.

Spatial coherency

The spatial coherency of the microtremor was also investigated and compared with that of the earthquake ground motion during the event #9. The coherence functions between boreholes P1 and P3, which are 30 m apart, and between boreholes C0 and P5, which are 124 m apart, were calculated as shown in Figure 16. Note that in the microtremor observation these station pairs were measured simultaneously. The coherence

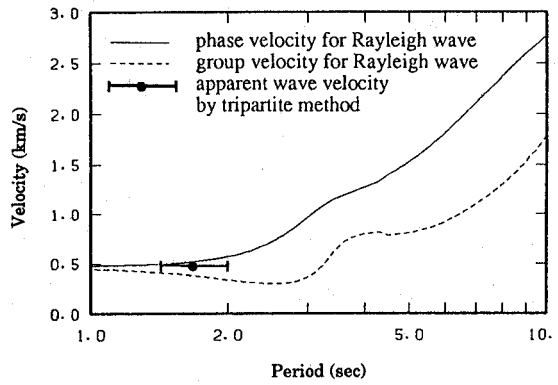

Figure 15. Comparison of theoretical dispersion curve and calculated apparent wave velocity from microtremor

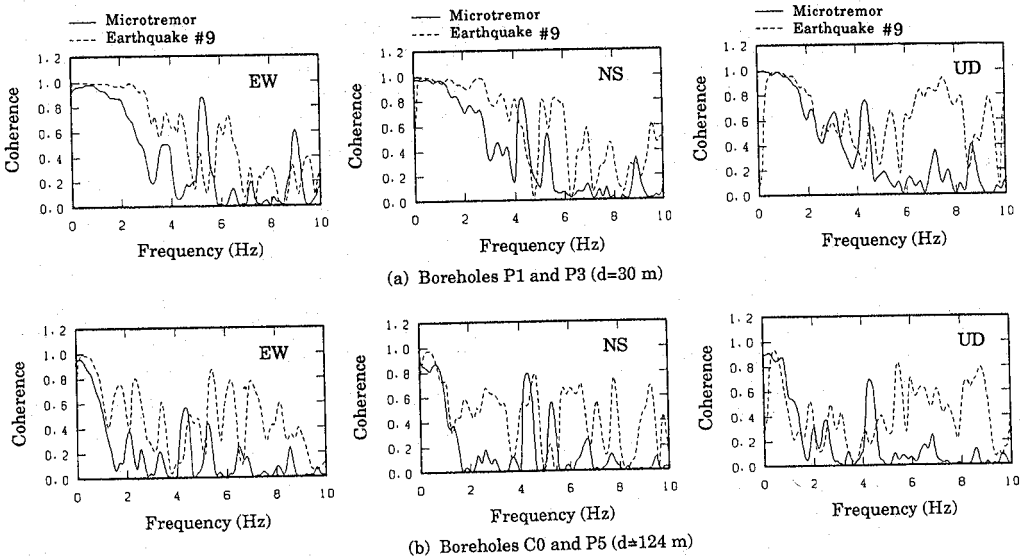

Figure 16. Comparison of coherence functions from microtremor and earthquake ground motion

function for the microtremor decreases as the frequency increases and as the separation distance increases. The coherence function for the earthquake shows the same tendency. However, the coherence function for the microtremor decreases more rapidly than that for the earthquake. The coherence function for the microtremor is high only in very low frequency contents. At high frequencies, the microtremor becomes spatially incoherent. In the case of earthquake ground motion, the higher frequency contents also consist of coherently travelling waves.

CONCLUSIONS

Amplification characteristics of earthquake ground motion were investigated in terms of peak ground acceleration and transfer function based on the Chiba array records. The amplification of the peak acceleration took place mostly within several metres below the ground surface. The amplification ratio at GL − 1 m was almost the double of the value at GL − 5 m. This contrasted strongly with the near absence of amplification from GL − 40 to GL − 20 m. The amplification of the vertical component is observed to be rather close to those of the horizontal ones.

Transfer functions were calculated by ensemble average for 16 events and by a smoothing procedure for individual events. The transfer functions from the ensemble average were very close for the two horizontal components while those from smoothing showed some difference for the two horizontal components. Valleys near the natural frequencies were found in the transfer functions from both the ensemble average and the smoothing operation. A two-step smoothing procedure, which estimates the amplitude of the transfer function by separating the mean phase angle, was proposed. The rotary spectrum was employed further to improve the estimation of the transfer function. It is believed that the resulting transfer function represents more realistic soil amplification characteristics than that obtained from the conventional procedure.

A microtremor was also observed at the locations of boreholes of the Chiba array. The power spectra of the microtremor were very close for the three components. For the earthquake ground motion, the power spectrum of the vertical component differed markedly from those of the two horizontal components. The peak around 0·4–0·6 Hz in the microtremor may be due to the Rayleigh wave because the measured apparent velocity coincided with the theoretical phase velocity of the Rayleigh wave. The peak around 2·5 Hz seen in the microtremor was believed to be caused by the S-wave propagating upward, since, at this frequency, the

peak was also observed for earthquake events. Hence the same local site effect could be seen in both the microtremor and earthquake ground motion around this frequency.

Although only the records from the Chiba array were examined, the methods used in this study can be applicable to other array observations and microtremor observations. Further studies using other data may be required until more general comments on soil amplification are made.

ACKNOWLEDGEMENTS

The authors express their sincere appreciation to Dr S. Nagata of the Institute of Industrial Science, the University of Tokyo and to Mr N. Sato of Tokyo Sokushin Co. Ltd for their collaboration in conducting the microtremor observation.

REFERENCES

1. V. Bertero, 'The 19 September 1985 Mexico earthquake: Building behavior', *Report No. EERC* 86-08, Earthquake Engineering Research Center, University of California, Berkeley, CA, 1989.
2. H. B. Seed *et al.*, 'Relationships between soil conditions and earthquake ground motions in Mexico City in the earthquake of Sept. 19, 1985', *Report No. EERC 87-15*, Earthquake Engineering Research Center, University of California, Berkeley, CA, 1987.
3. L. Benuska *et al.*, 'Loma Prieta earthquake reconnaissance report', *Earthquake Spectra* **6** supplement (1990).
4. R. Seed *et al.*, 'Preliminary report on the principal geotechnical aspects of the October 17, 1989 Loma Prieta earthquake', *Report No. EERC 90-05*, Earthquake Engineering Research Center, University of California, Berkeley, CA, 1990.
5. S. Omote *et al.*, 'Observation of earthquake strong-motion with deep boreholes: An introductory note for Iwaki and Tomioka observation station in Japan', *Proc. 8th world conf. earthquake eng.* San Francisco **2**, 247–254 (1984).
6. Y. Kitagawa, I. Ohkawa and T. Kashima, 'Dense strong motion earthquake seismometer array at site with different topographic and geologic conditions in Sendai', *Proc. 9th world conf. earthquake eng.* Tokyo-Kyoto **2**, 215–220 (1988).
7. H. Tang *et al.*, 'A large-scale soil–structure interaction experiment: Design and construction', *Nucl. Eng. des.* **111**, 371–379 (1989).
8. C. Real and C. Cramer, 'Turkey Flat, USA, site effects test area: "Blind" test of weak-motion soil response prediction', *Proc. 4th U.S. nat. conf. earthquake eng.* Palm Springs, CA **1**, 535–544 (1990).
9. S. Kurita, M. Izumi, S. Iizuka, T. Sato and T. Aiba, 'Statistical characteristics of seismic wave propagation in soil with vertical instruments array', *Proc. 9th world conf. earthquake eng.* Tokyo-Kyoto **2**, 515–520 (1988).
10. K. Kanai and T. Tanaka, 'On microtremors, VIII', *Bull. earthquake res. inst.* **39**, 97–114 (1961).
11. Y. Osawa *et al.*, 'Estimation of structural damage based on the effect of local surface geology', *Proc. 9th world conf. earthquake eng.* Tokyo-Kyoto **2**, 453–458 (1988).
12. H. Kagami *et al.*, 'Observation of 1 to 5 s microtremors and their application to earthquake engineering, Part II: Evaluation of site effect upon seismic wave amplification due to extremely deep soil deposits', *Bull. seism. soc. Am.* **76**, 987–998 (1982).
13. C. Loh, G. Su and C. Yeh, 'Development of stochastic ground movement: Study on SMART-1 array data', *Soil dyn. earthquake eng.* **8**, 22–31 (1989).
14. T. Katayama, F. Yamazaki, S. Nagata, L. Lu and T. Turker, 'A strong motion database for the Chiba seismometer array and its engineering analysis', *Earthquake eng. struct. dyn.* **19**, 1089–1106 (1990).
15. T. Turker, F. Yamazaki and T. Katayama, 'Analysis of seismic wave propagation based on the Chiba array database', *Proc. 8th Japan earthquake eng. symp.* **1**, 505–510 (1990).
16. J. Bendat and A. Piersol, *Random Data: Analysis and Measurement Procedures*, Wiley, New York, 1971.
17. L. Lu, F. Yamazaki and T. Katayama, 'Soil amplification based on the Chiba array database', *Proc. 8th Japan earthquake eng. symp.* **1**, 511–516 (1990).
18. J. Gonella, 'A rotary-component method for analyzing meteorological and oceanographic vector time series'. *Deep-sea res.* **19**, 833–846 (1972).
19. J. Lysmer, 'Lumped mass method for Rayleigh waves', *Bull. seism. soc. Am.* **60**, No. 1 (1970).